Journal of the Korean Physical Society, Vol. 70, No. 7, April 2017, pp. 682∼686

Construction and Performance Test of Prototype Parallel Plate Avalanche Counters at RAON

Charles Akers,* Kwang Bok Lee, Young Jin Kim, Eun Hee Kim, Young Kwan Kwon, Hyo Sang Lee, Jun Young Moon, Jin Hyung Park, Min Sang Ryu, Taeksu Shin and Satou Yoshiteru
Rare Isotope Science Project, Institute for Basic Science, Daejeon 34047, Korea

(Received 9 November 2016, in final form 13 February 2017)

Two prototype position sensitive parallel plate avalanche counters (PPACs) have been fabricated at the Rare Isotope Science Project (RISP). Both detectors have active areas of 10 × 10 cm^2 and utilize a stripped electrode structure, together with a delay line readout, to extract position information. Testing was conducted with an ^{241}Am α source, and 2-dimensional position information was obtained. A position resolution of 0.55 mm full width at half maximum (FWHM), together with a position linearity of ±55 μm over a 67-mm detection range, were measured. A time resolution of 450 ps (FWHM) was also measured.

PACS numbers: 29.40.Cs, 29.40.Gx
Keywords: PPAC, RISP, RAON, Position sensitive, delay-line readout
DOI: 10.3938/jkps.70.682

I. INTRODUCTION

Parallel plate avalanche counters (PPACs) represent a simple, yet effective, mechanism for beam diagnostics and particle identification of rare isotope (RI) beams. They exhibit many desirable properties: good position and timing resolution, high efficiency, high detection rate capability, resistance to radiation damage, simple, cost effective design, and minimal perturbation of incident-beam ions. PPACs have also been under development for over 50 years [1]; thus, they constitute a proven, established means of ion detection. Such detection devices are required for the planned in-flight (IF) separator [3] and KOBRA spectrometer [2], which will generate secondary RI beams at around 20 MeV/nucleon. As a range of nuclear species will be produced in the secondary beam, particle identification (PID) is needed on an event-by-event basis if specific reactions are to be measured successfully.

PPAC detectors comprise two flat parallel-plane electrodes, one of which is biased, forming a strong linear electric field ($\gtrsim$ 100 V/mm). A quencher gas is then flowed through the gap between the electrodes. In this way, incident ions traversing the region of sensitive-gas may form primary electrons via the ionization of the gas molecules present within the detector. This results in the creation of a Townsend electron avalanche directed orthogonally towards the anode plane [4]:

$$N_e = N_0 e^{\alpha z}, \quad (1)$$

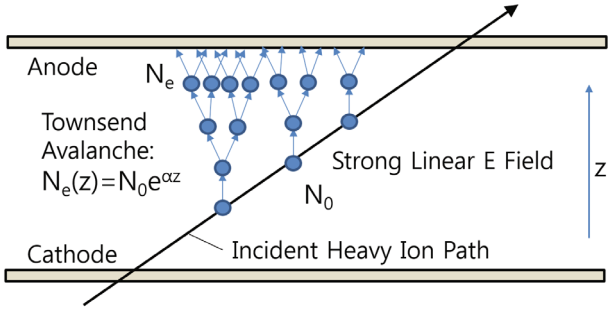

Fig. 1. (Color online) Diagram showing the basic priciple of avalanch generation in PPAC detectors.

where N_e is the number of electrons in the avalanche, N_0 is the number of primary electrons, z is the distance normal to the electrode's surface and α is the first Townsend coefficient. α^{-1} represents the mean free path between ionization events, typically $\approx$ 0.3 mm in PPAC designs [5]. This exponential increase in the number of election-ion pairs allows for large electron gain values of up to approximately 10^5. Figure 1 provides an illustration of this process.

As electrons have a much greater drift velocity than their ion counterparts, the induced current on the electrodes exhibits a sharp initial peak, approximately 10 ns in width, due to the fast moving electrons being rapidly swept towards the anode. A lower, but much longer component, approximately 1 μs long, due to the slower moving ions drifting towards the cathode follows. The fast electron component of the signal alone can be used to ex-

*E-mail: cakers@ibs.re.kr

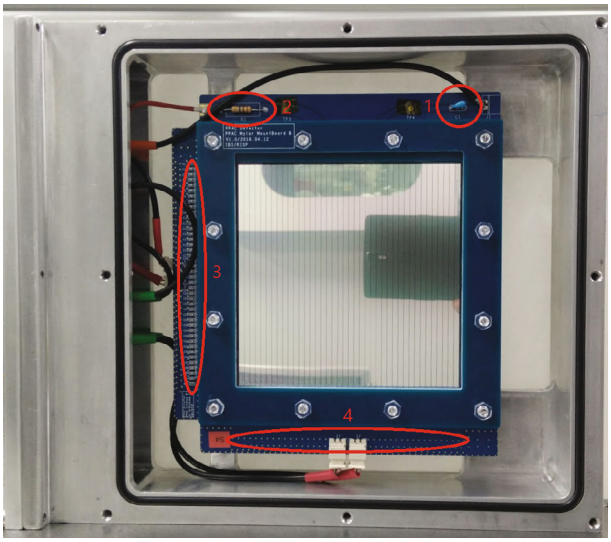

Fig. 2. (Color online) Photograph of the PPAC case with the front window frame removed. The stripped structure of the x cathode can be seen. The x and the y delay lines are also visible (labelled as (4) and (3), respectivly), as are the anode resistor (2) and capacitor (1).

tract both timing and position properties and can result in PPAC detectors achieving very high detection rates of over 10^6 particles per second [6]. Unlike other types of proportional counters, in PPACs, only approximately 10% of the total induced signal appears in the form of the fast electron component; the majority of the signal comprises the slow ion tail. This makes noise reduction and signal amplification especially important for PPAC detection systems that rely on the fast electron signal for position measurements [6].

II. DESIGN AND CONSTRUCTION

The PPAC electrodes consist of thin (2-μm) Mylar sheets, 10 × 10 cm^2 in area, tightly stretched and attached to supporting FR4 frames with epoxy. Each detector is comprised of three electrodes: a central anode electrode located between two outer orthogonally stripped cathode electrodes. The entire gas volume is contained between two 4-μm aluminized Mylar windows supported by an aluminum case (see Fig. 2). The central anodes were formed by evaporating 30 nm of Al onto both sides of the Mylar sheets. For the cathodes, metal electroformed masks were mounted onto the frames, after which 30 nm of Ag was evaporated onto their surfaces, to produce their strip structure. The evaporation work was performed using an E-beam evaporator at the National Nano-Fab Center (NNFC). Each stripped cathode has 40 strips, 2.35 mm in width and separated by a 0.15-mm space (see Fig. 2). A 4-mm gap is kept between the electrodes by using G10 spacers between the Mylar

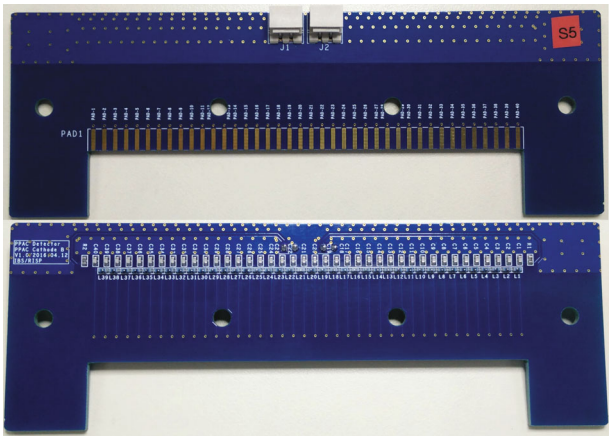

Fig. 3. (Color online) Photographs displaying both sides of the PPAC delay-line boards. The top photo shows the front side, with the gold plated contacts used for electrical contact with the stripped cathode Mylar sheet visible. The lower photo displays the rear side of the delay board, with the individual capacitor and inductor elements visible.

frames.

Position data on both the x and the y axes are extracted from the cathodes via two discrete LC element delay lines (see Ref. [7]), grounded through 500-kΩ resistors, one each at either end. Each delay board has a calculated characteristic impedance of 48 Ω and a measured 2.0-ns delay per tap. Each tap comprises a 0603-chip-size 91-nH inductor (2% tolerance) and a 39-pF capacitor (1% tolerance). Thirty nine taps, which are mounted on a separate frame to the electrodes so that they do not need to be discarded every time the Mylar sheets are damaged and replaced, compose each delay line. Electrical contact is kept between the delay-line contacts and the electrode by the mechanical pressure exerted from a hollow Si tube. See Fig. 3 for photographs of the delay-line boards. Adopting a delay of ≈1 ns/mm means that the signals induced in neighboring electrode strips are summed such that the total signal waveform remains relatively unchanged as a function of incident ion position. This allows for the detector's position resolution to be much more precise than the electrode-strip's width [8].

Position measurements are extracted by splitting the electrode time signals so that each signal is readout from both extremities of the delay line. The relative time difference between the two split-signals then gives a measure of position along the electrode plane:

$$x = k(T_2 - T_1) + x_0, \tag{2}$$

where x is the linear position along the electrode plane; T_1 and T_2 are the measured time delays of the two split electrode signals; k is the coefficient for converting the time difference between T_1 and T_2 to position; and x_0 is the position offset. This formalism is advantageous as the position measurement is a function of the electrode time signals only; any dependence on the timing resolution of other components is removed.

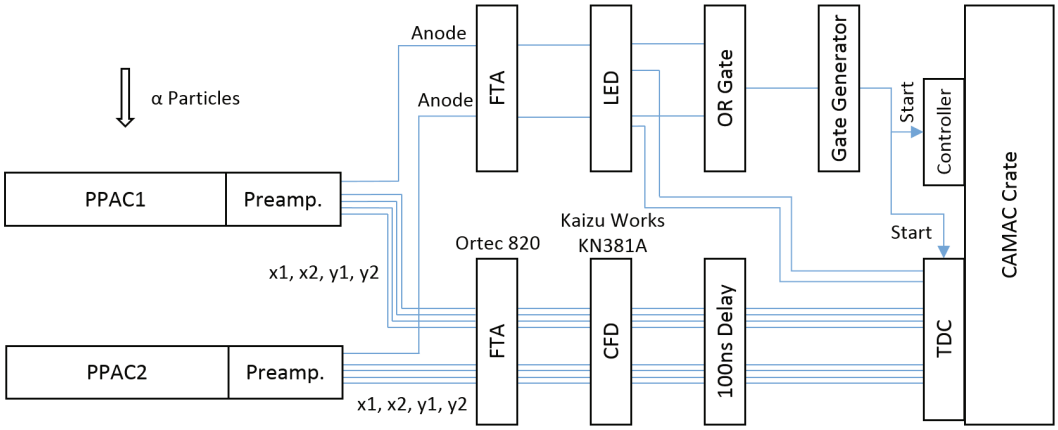

Fig. 4. (Color online) Electronics and DAQ setup used for the position measurements and the efficiency tests. For the TOF measurements, the Ortec FTA was used for the anode signals and a CFD instead of the LED, was used for timing.

III. EXPERIMENTAL TESTING AND RESULTS

The detectors were operated with 4 to 15 Torr of quencher gas, either C_3F_8 or C_4H_{10}, at a flow rate from 3 to 6 SCCM (standard cubic centimeters per minute). These two gasses were used due to their ease of operation and high gain values. A positive bias was applied to the central anode though a 10-MΩ resistor, forming an electric field of a few hundred $\mathrm{Vcm^{-1}Torr^{-1}}$ in the avalanche region between the electrodes. The resulting anode signals were filtered through a 220-pF capacitor, which protected the pre-amplifier from the anode's high DC voltage. The stability of the gas pressure was maintained via an inlet mass-flow controller and outlet needle valve. The PPACs were tested with an ^{241}Am 5.5-MeV α source. Signal amplification was done using fast, low noise charge sensitive preamplifiers and a fast timing amplifier (FTA) with a gain of 200. Constant fraction discriminators (CFDs) were used to obtain precise timing information, and a CAMAC time-to-digital converter (TDC) was used for data acquisition. Figure 4 outlines the electronics in more detail.

The position resolution was measured by mounting slits onto the cathode frames in the detector. This allowed for good collimation in the sensitive-gas region. The slits had a width of 0.5 mm and a pitch of 2.5 mm, such that every cathode strip corresponded to a single slit. An example of one such resulting position spectrum is given in Fig. 5. The best performance and gas stability were found at a gas pressure of 10 Torr. Position calibration involved fitting Gaussian peaks to the position spectra and recording their centroid and standard-deviation values. As each peak corresponded to a single slit, the peak-to-peak centroid separation corresponded to the slit pitch, so that a TDC channel-to-linear-distance conversion factor could be calculated, which corresponds to the constant k in Eq. (2). This method involved plotting the peak centroid TDC values against the corresponding

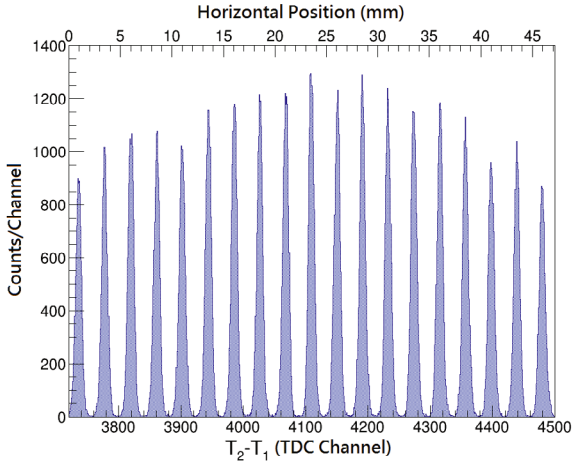

Fig. 5. (Color online) Position spectrum resulting from a 0.5-mm-wide slit mask with a 2.5-mm pitch mounted on the x cathode. The top axis displays the calibrated horizontal scale (see the text for the details).

slit's horizontal positions, in mm, and fitting a straight line to the data. The gradient of this fit then provided a factor for converting the TDC channel to a linear distance, k. An example of a TDC peak centroid to position conversion plot is given in Fig. 6.

Once the conversion factor k had been calculated, the detector's position resolution could be inferred from standard deviation values (σ_{fit}) for the aforementioned fitted Gaussian peaks. These σ_{fit} values were a result of both the geometric width of the slits (σ_{geom}, which was taken as the route-mean-square of a uniform distribution of 0.5-mm width, 0.144 mm, rather than the width of the slits) and the intrinsic resolution of the PPAC and electronics (σ_{PPAC}); hence, σ_{PPAC} could be calculated from

$$\sigma_{\mathrm{fit}}^2 = \sigma_{\mathrm{geom}}^2 + \sigma_{\mathrm{PPAC}}^2. \quad (3)$$

Using this method, an intrinsic position resolution of

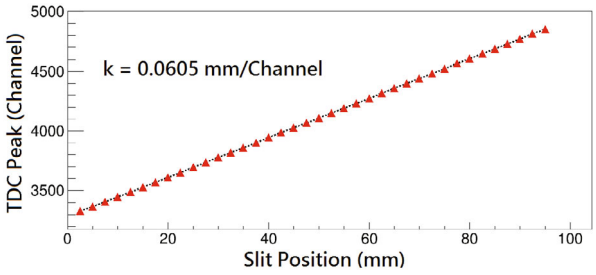

Fig. 6. (Color online) Position calibration graph. The centroid values of the fitted Gaussian peaks are plotted against slit position, yielding a strong linear relationship. The fitted line (shown as dashed) yields a gradient of 16.5 channels/mm, coresponding to $k = 0.0605$ mm/channel, which is then used as a conversion from TDC channel to horizontal position (see the text for the details).

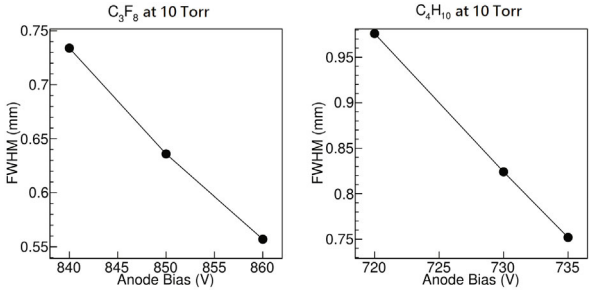

Fig. 7. Graphs showing how the intrinsic position resolution of the PPAC detectors and thier accociated electronics, in FWHM, improved as the anode bias voltage was increased.

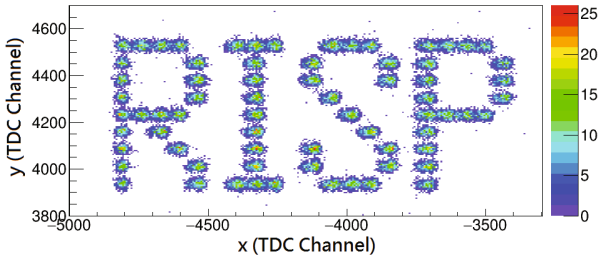

Fig. 8. (Color online) Two-dimensional position spectrum with a 2-mm-diameter circular array mask mounted onto the x cathode. In this case, C_4H_{10} at 10 Torr was used with an anode bias of 730 V.

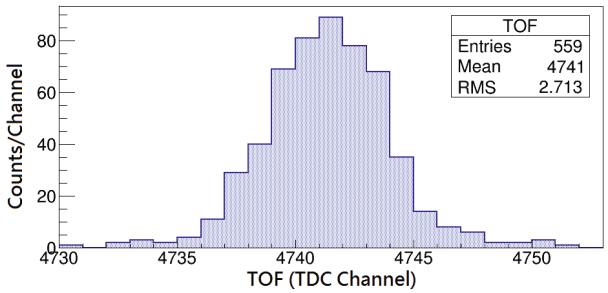

Fig. 9. (Color online) Time-of-flight spectrum for both PPAC detectors with 4.5 Torr of C_3F_8 gas. The data's RMS was used to extract the timing resoluton (see the text for the details).

0.55 mm FWHM was observed, together with a position linearity (defined here as the difference between the fitted peak's centroid and the corresponding slit center position) of $< \pm 55$ μm over a 67-mm range, when using the C_3F_8 gas. The operational anode bias was determined by increasing it incrementally until the leakage current became unstable. Position resolution was observed to improve significantly at higher voltages, as seen in Fig. 7. Hence, operating at higher voltages stably is of primary concern when considering the PPAC design. The 2-dimensional capability of our PPACs is also illustrated in Fig. 8, where a patterned mask was mounted for this purpose.

Time-resolution and efficiency measurements were conducted with both PPACs mounted sequentially along the trajectory of the incident α particles, with both detectors using the same gas flow system in parallel. The efficiency of PPAC1, closest the source, was calculated via

$$\epsilon_1 = \frac{N_{1\&2}(x)}{N_2(x)}, \tag{4}$$

where $N_2(x)$ is the number of events detected with a valid position in the second PPAC and $N_{1\&2}$ is the number of events with a valid position in both detectors. High efficiencies, of over 99%, were calculated for both gases.

The detector's time resolution was calculated via a time-of-flight (TOF) measurement between the two detectors. The central-electrode's bias polarity was reversed for the TOF measurements so that a better performance FTA (Ortec 820) could be used for central electrode signal processing, as it could only accept negative-polarity signals (a positive bias on the central electrode generated a positive-polarity output signal after having passed through the inverting preamplifier). The detectors were found to operate better at a lower pressure, 4.5 Torr, when a negative bias was applied. The fast components of the central-electrode signals were used for timing information, and a 2-mm-diameter circular collimator was placed on the face of PPAC1 so as to limit the geometrical spread of α-event trajectories. This meant that the spread in the TOF spectrum was due primarily to the intrinsic timing resolution of the PPAC and associated electronics. The resulting TOF peak is given in Fig. 9. The TDC was measured to have a calibration of 100 ps/channel, giving the TOF distribution a route-mean-square of 270 ps (rounding to 2 significant figures). If we consider both PPACs to have an equal time resolution, then dividing this number by $\sqrt{2}$ yields the resolution of an individual detector: 190 ps. This is 450 ps FWHM if we approximate the timing distribution to be a Gaussian distribution. Analysis of the Stopping Range of Ions in Matter (SRIM) database [9] suggested

Table 1. Results of the ^{241}Am α source test measurements with both gases. Resolutions are presented in FWHM.

Property	C_3F_8	C_4H_{10}
Central electrode bias	860 V	735 V
Gas pressure	10 Torr	10 Torr
Position resolution	0.55 mm	0.75 mm
Efficiency	$> 99\%$	$> 99\%$
Central electrode bias	-660 V	-540 V
Gas pressure	4.5 Torr	4.5 Torr
Time resolution	450 ps	520 ps
Signal rise time	6 ns	6 ns

that approximately 50% more energy was deposited in PPAC2 than PPAC1, which may mean that the former had a better time resolution due to the stronger anode signals afforded by greater primary-electron generation. In this case, the quoted resolution is still valid, but represents an upper limit. A summary of the performance results for both gases is given in Table 1.

IV. SUMMARY AND OUTLOOK

Two prototype position-sensitive PPACs have been fabricated for use with the KOBRA spectrometer and IF separator, as part of the RISP project. A strip, segmented, cathode structure, coupled with a discrete LC element delay line, enabled position information to be extracted from the electrode's fast-electron-induced signals. Both detectors had a sensitive area of 10×10 cm^2 and operated best with C_3F_8 gas. When tested with a ^{241}Am 5.5-MeV α source, the detectors exhibited good position and time resolution (0.55 mm and 450 ps FWHM, respectively), as well as a high efficiency ($> 99\%$), together with a position linearity of ± 55 μm over a 67 mm detection range.

In the future, we hope to test these detectors more thoroughly at a beam facility so that their performance can be characterized when using various ion species at different beam energies and intensities. We have also finished fabricating a much larger PPAC detector with a sensitive area of 20×20 cm^2 and are currently testing its performance. Plans for a PPAC detector with an even larger active area, to accommodate the large beam spreads anticipated at KOBRA, are currently underway.

ACKNOWLEDGMENTS

This work has been supported by the Rare Isotope Science Project and by the Institute for Basic Science, with funding provided by the Ministry of Science and the National Reference Foundation (NRF) of Korea (2013M7A1A1075765).

REFERENCES

[1] J. E. Draper, Nucl. Instrum. Meth. **30**, 148 (1964).
[2] K. Tshoo, H. Chae, J. Park, J. Y. Moon, Y. K. Kwon, G. A. Souliotis, T. Hashimoto, C. Akers, G. P. A. Berg, S. Choi, S. C. Jeong, S. Kato, Y. K. Kim, S. Kubono, K. B. Lee and C. B. Moon, Nucl. Instrum. Meth. B **376**, 188 (2016).
[3] A. Zaghloul, Y. J. Kim, D. G. Kim, H. C. Jo and M. J. Kim, J. Korean Phys. Soc. **67**, 1422 (2015).
[4] H. Stelzer, Nucl. Instrum. Meth. **133**, 409 (1976).
[5] M. Nakhostin, Nucl. Instrum. Meth. A **615**, 53 (2010).
[6] H. Kumagai, A. Ozawa, N. Fukuda, K. Summerer and I. Tanihata, Nucl. Instrum. Meth. A **470**, 562 (2001).
[7] D. Harrach and H. J. Specht, Nucl. Instrum. Meth. **164**, 477 (1979).
[8] H. Kumagai, T. Ohnishi, N. Fukuda, H. Takeda, D. Kameda, N. Inabe, K. Yoshida and T. Kubo, Nucl. Instrum. Meth. B **317**, 717 (2013).
[9] J. F. Ziegler, M. Ziegler and J. Biersack, Nucl. Instrum. Meth. B **268**, 1818 (2010).